ISSN 2616-5767 Vol.8, Issue 1: 73-80, DOI: 10.25236/AJETS.2025.080111

High-Q all-dielectric metasurface refractive index sensor based on quasi-BICs

Wang Junhui

School of Physics and Electronic Science, Hunan University of Science and Technology, Xiangtang, Hunan, China

Abstract: *Bound states in the continuum (BICs) are ideal for realizing optical resonances with ultra-high quality factors (Q) because of their extreme ability to facilitate light-matter interactions and strong field confinement. In this work, an all-dielectric metasurface whose unit cell consists of a silicon disc is designed, on which a symmetry-protected BIC (SP-BIC) is observed, and the breaking of the in-plane symmetry can be made to transform it into a quasi-BIC (QBIC) with a high-quality factor. A refractive index sensor is realized based on the principle that the resonance peak's position changes with the background refractive index change. Using the quadratic inverse relationship between the quality factor and the asymmetry parameter, the quality factor is changed by adjusting the asymmetry parameter to optimize the sensing performance. After tuning, the refractive index sensing sensitivity and figure of merit of this metasurface reached 265.58 nm/RIU and 2178.31 RIU-1, respectively, a parameter that exceeds many existing research results. This all-dielectric metasurface design with a high Q-factor pushes the BIC-based refractive index sensing to higher sensitivity and higher accuracy.*

Keywords: *all-dielectric metasurface, bound states in the continuum, refractive index sensing*

1. Introduction

Waves that are completely confined in the continuum spectrum of radiated waves without interacting with them are known as bound states in the continuum (BICs), which are a unique type of fully confined modes [1,2]. The concept of BICs originally originated in quantum mechanics and has since been extensively studied in different fields of fluctuation physics, including acoustics, microwaves, water waves, and nanophotonics[3–5]. In 2008, the concept of BIC was first introduced into the field of optics[6]. Since then, various optical structures such as thin nanophotonic crystals, optical waveguide arrays, and metasurfaces have been successively realized with high Q-factor resonance by BIC[7,8]. The ideal BIC is completely decoupled from the free-space radiation with a theoretically infinite quality factor, and the radiation lifetime tends to infinity [9], which is manifested spectrally by the disappearance of the resonance linewidth of the Fano resonance. According to the physical mechanism of decoupling, BICs can be divided into two categories: accidental BICs, in which the continuous adjustment of system parameters leads to accidental decoupling[10,11], and symmetry-protected BICs (SP-BICs), in which discrete modes and continuous radiation modes are decoupled due to the breaking of spatial symmetry[12]. In photonic crystal slabs, modes above the light with structure are usually radiative due to coupling to the continuum of extended modes. However, due to the symmetry mismatch between their mode profiles and the external propagation modes, certain bound states can exist even above the light of the band structure. At the Γ point of the photonic crystal energy band, when the operating frequency is below the diffraction limit, the only radiating state is a normal plane wave [13], whose electromagnetic field distribution is singular, i.e., C_2-symmetric, under a 180° rotation about the z-axis, and thus any even modes at the Γ point are BICs[14]since the overlap between their mode distribution and the outgoing wave is zero. Since SP-BICs are more common and easy to implement, they have been found in various photonic micro- and nanostructures such as waveguides [15,16], gratings[17], and metasurfaces[18]. Symmetry-protected BICs are ideal BICs that do not radiate energy outward and have zero linewidth, and therefore cannot be detected in the spectrum. In practical applications asymmetric factors are usually introduced into the system to break the symmetry of the structure leading to coupling between the SP-BIC and the continuum radiation, creating a radiation channel that transforms the SP-BIC into a quasi-BIC (QBIC). The QBIC can be considered as a leakage mode occurring in the vicinity of the BIC with a finite but large Q-factor, which is manifested in the transmission spectrum as having a sharp Fano line shape in the transmission spectrum. At the same time, it can be directly excited by an external light source without a special coupling mechanism. Currently, the QBIC mechanism has been used in various

ISSN 2616-5767 Vol.8, Issue 1: 73-80, DOI: 10.25236/AJETS.2025.080111

applications such as filters[19], lasers [20], nonlinear devices[14], and sensors [21].

In the last decade, metasurfaces have attracted significant attention due to their easy tunability and notable robustness. Among these, conventional noble metal-based metasurfaces inevitably exhibit low Q-factors because of the inherent issue of high ohmic losses[22,23]. In contrast, all-dielectric metasurfaces are anticipated to serve as an excellent alternative to plasma-based metasurface structures, thanks to their flexible tunability, low ohmic loss, strong localization, and ultra-compact design. To date, many metasurface structures supporting QBIC high-Q resonance have been proposed, such as tilted dielectric ridges[24], dielectric split rings [25], and unequal-scale dielectric cubes[26]. In practical applications, optical sensing, which relies on changes in spectral shape, resonance wavelength, and the intensity of optical resonance caused by alterations in the dielectric environment, has been successfully demonstrated[27]. For QBICs formed on metasurfaces, the resonance wavelength typically shows a strong dependence on the refractive index of the surrounding environment due to the intense localization of the electric field within the cell[28], a property frequently utilized for optical sensing. The high Q-factor of QBICs can result in enhanced sensitivity and a greater figure of merit for optical sensors.

In this paper, a structure of an all-dielectric metasurface refractive index sensor supporting a high Q-factor QBIC resonance whose leaked radiation is dominated by an electric quadrupole (EQ), which can have a Q-factor of more than 105 under specific conditions is proposed. By breaking the symmetry of the in-plane structure, the SP-BIC transforms into a QBIC with an ultra-high Q-factor, accompanied by a The SP-BIC is transformed into QBIC with ultra-high Q-factor by breaking the symmetry of the in-plane structure, which is accompanied by huge local field enhancement. At the same time, it has lower ohmic loss and higher tunability than conventional plasma metasurfaces. By controlling the value of the asymmetry parameter, the spectral linewidth of the QBIC mode can be flexibly controlled, and the sensing performance can be enhanced and tuned. Through tuning, the sensitivity and figure of merit can be as high as 265.58 nm/RIU and 2178.31 RIU^{-1}, which are higher than many published results based on other conventional methods. The high FOM sensing performance endows the sensor with higher accuracy to detect small refractive index changes more precisely, thus providing more reliable detection results, as can be seen from the excellent performance of this QBIC-based refractive index sensor. In addition, the simple design allows the sensor to be adapted to a variety of complex detection environments, expanding its application prospects in a variety of refractive index sensing areas.

2. Structural design and simulation

The minimum structural unit of the designed all-dielectric metasurface structure is shown in Figure 1. Silicon nanodisks with radius R=300nm and height h=100nm are placed on a glass substrate with a thickness of 1000nm. The periodic dimension of the structural unit is Px=Py=700nm. The in-plane symmetry of the structure is broken by introducing an eccentric hole of variable radius r at a fixed distance of 150nm from the center of the nanodisc, as schematically shown in Figure 1(b). The in-plane symmetry is broken, allowing the establishment of radiation channels and the transition of the resonance state from a symmetry-protected BIC to a quasi-BIC.The simulations are carried out in the commercial software Lumerical FDTD Solutions, and the numerical simulations are performed using the finite-difference time-domain (FDTD) method, which is an effective means of providing accurate predictions for electromagnetic interaction problems [29]. The light source of the system is set to be a near-infrared plane wave between 1090 nm and 1250 nm incident along the -z-axis, and the electric and magnetic fields are polarised along the y and x axes, respectively, so that a periodic boundary condition is applied in the x-y plane and a perfectly matched layer is used in the z-direction. To simplify the simulation, the refractive indices of silicon and glass are set to 3.53 and 1.45 respectively, and the background is set to a uniform background with a refractive index of 1.

ISSN 2616-5767 Vol.8, Issue 1: 73-80, DOI: 10.25236/AJETS.2025.080111

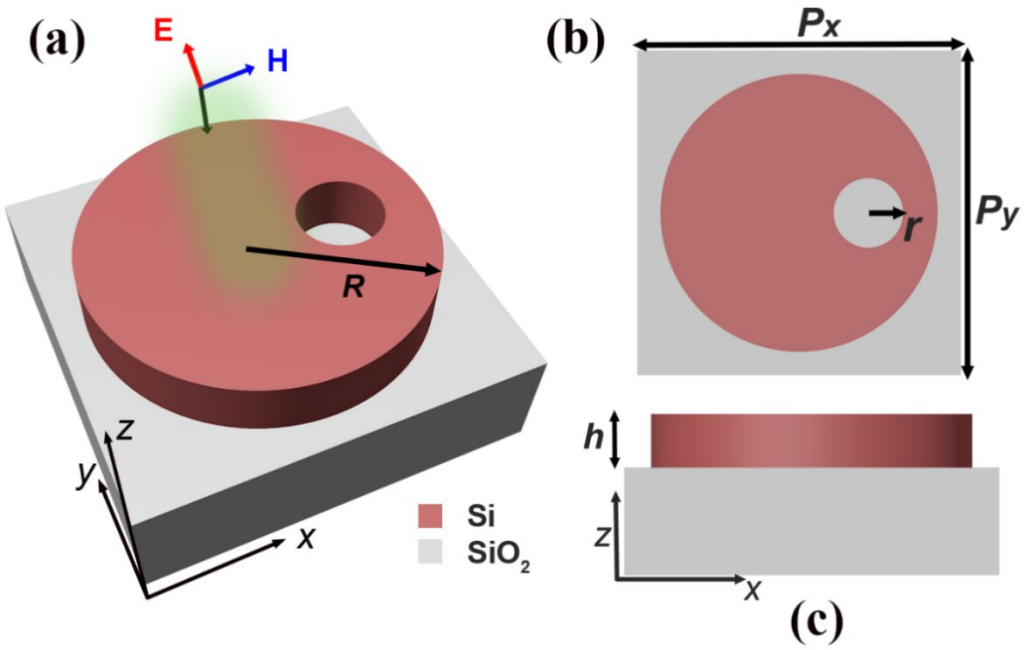

Fig. 1 (a) Schematic of the proposed all-dielectric metasurface. The structural parameters are Px=Py=700nm, R=300nm, h=100nm, and the thickness of the glass substrate is set to 1000nm. (b) An off-centered hole with variable radius r is introduced at a fixed distance of 150nm from the center of the disc to break the C2 symmetry of the structure. (c) Front view of the silicon nanodisc metasurface.

As shown in Figure 2(a), the first consideration is a substrate-free C_2-symmetry silicon nanodisk consisting of ideally independent periodic arrays. To search for the BIC, all possible resonance modes supported by the periodic array were excited using a dipole cloud[30], and the resulting photonic band structure is shown in Figure 2(b). The position of the SP-BIC is marked with a red circle in the figure at the Γ point of the first Brillouin zone and lies in the near-infrared-II (NIR-II) frequency range. Its corresponding frequency is below the diffraction limit for a given periodic structure, and the only radiation channel in this case is a plane wave propagating along the normal direction[12]. The electromagnetic field vector of the SP-BIC mode is singular under C_2-symmetry, and due to the symmetry mismatch the resonance modes are completely confined and no longer coupled to the other radiation channels in free space, leading to the theoretically infinite Q-factor[31,32]. If a defect is introduced to break the in-plane symmetry, the radiation channels are opened, transforming the SP-BIC into a QBIC with a finite and large Q-factor and a distinct Fano signature in the optical response spectrum.

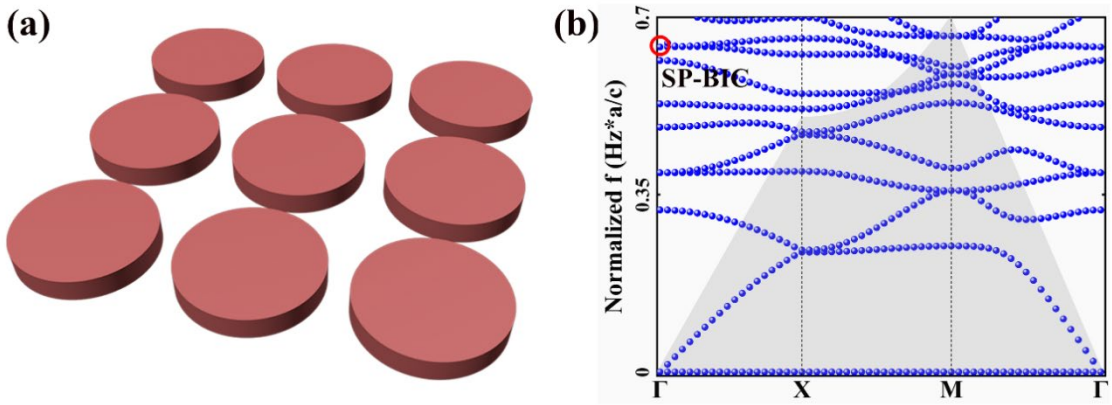

Fig. 2 (a) Schematic of a metasurface consisting of periodically aligned arrays of silicon nanodiscs. (b) Calculated photonic bandstructure of the periodically aligned silicon nanodisk array in (a).Grey shading indicates the region located below the free-space light cone. The location of the trapped symmetrically protected BIC is marked with a red circle.

In practice, the periodically aligned silicon nanodiscs need to be placed on a substrate, so here a glass substrate with a low loss index is introduced, and the presence of the substrate causes a small amount of bound energy to leak out of the open radiation channels in the substrate, which in turn leads

ISSN 2616-5767 Vol.8, Issue 1: 73-80, DOI: 10.25236/AJETS.2025.080111

to a decrease in the Q-factor as well as a change in the resonance position [33]. However, the SP-BIC supported by the proposed structure is quite robust[34] and the presence of the substrate does not have a significant effect. The QBIC resonance is closely related to the radiation leakage and therefore the radiation rate and transmission linewidth can be tuned by controlling the geometrical parameters. The linewidth of the transmission spectrum at the QBIC resonance gradually increases as the radius of the eccentric aperture increases. To demonstrate this SP-BIC to QBIC transition more intuitively, the transmission spectra with variation of the eccentric aperture radius are calculated as shown in Figure 3(a). From the figure, it can be seen that the transmission line width is also zero when the eccentric hole radius r is 0. This means that the resonance peak disappears and there is no energy leakage from the bound state to the free space continuum, corresponding to a theoretical infinity of the Q-factor. In contrast, as r increases, the transmission slope is slightly blueshifted and broadened, and the QBIC exchanges energy with the continuous free space radiation mode, manifesting as a sharp Fano resonance [35]. As shown in Fig. 3(b), a single case of r = 75 nm is considered, from which the transmission spectrum shows an asymmetric line shape and a narrow dip at λ = 1093.44 nm, which agrees well with the Fano line shape in the classical coupled mode theory (CMT) framework, and to illustrate this the transmission spectrum is fitted using the classical Fano formulae [36,37]:

$$T(\omega) = T_0 + A_0 \frac{\left(q + 2\left(\omega - \omega_0\right)/\gamma\right)^2}{1 + \left(2\left(\omega - \omega_0\right)/\gamma\right)^2} \tag{1}$$

where ω_0 is the resonance center frequency, γ is the resonance line width, T_0 is the background scattering parameter, A_0 is the coupling coefficient between the continuous and discrete states, and q is the Breit-Wigner-Fano parameter which determines the asymmetry of the resonance curve, and $Q = \omega_0/\gamma$ can be calculated according to the fitting equation[32]. As shown in Fig. 3(d), the Q factor of the QBIC mode for different eccentric hole radius conditions is calculated and plotted as a functional correspondence with the asymmetry parameter, where the asymmetry parameter α is defined as the ratio of the area of the eccentric hole (noted as S_1) to the area of the original silicon wafer (noted as S_0):

$$\begin{aligned} \alpha &= \frac{S_1}{S_0} \\ &= \frac{r^2}{R^2} \end{aligned} \tag{2}$$

For a more intuitive visualization of the relationship between the Q-factor and the asymmetry parameter α, the coordinates are plotted on a $\log_{10}$-$\log_{10}$ scale, from which it can be seen that the Q-factor and α have a clear inverse quadratic relationship within a reasonable range[35]:

$$Q(\alpha) = Q_0[\alpha]^{-2} \tag{3}$$

where Q_0 is a constant determined by the metasurface structure, independent of the asymmetry parameter α. The results show that the Q-factor of the QBIC resonance supported by the silicon nanodiscs is regulated over three orders of magnitude with the variation of the radius of the eccentric pore, which can actively regulate the coupling efficiency and the magnitude of the Q-factor to a large extent, and at the same time, such a large Q-factor also provides a great application prospect for the realization of high-resolution optical biosensors. To further explore the radiative mechanism of the QBIC resonance, as shown in Figure 3(c), a multi-level decomposition of the scattering cross section by the optical resonance response at r = 75 nm [38,39], reveals that the QE has the largest radiative power and the contributions of all other polariton resonances are very weak, further suggesting that such a QBIC radiative state is dominated by the QE response, which represents the coupling to the outgoing wave in the system. Figure 3(e) shows the near-field distribution of the electric field in the corresponding x-y plane at r = 75 nm. It can be seen that the electric field is strongly enhanced at the eccentric hole, indicating that the incident light along the -z direction is strongly confined within the metasurface by the magnetic dipole oscillations, while the large Q-factor significantly enhances the local light-matter interaction. The superimposed arrows indicate the distribution of in-plane displacement currents, which is characteristic of electric quadrupole resonances[40,41].

ISSN 2616-5767 Vol.8, Issue 1: 73-80, DOI: 10.25236/AJETS.2025.080111

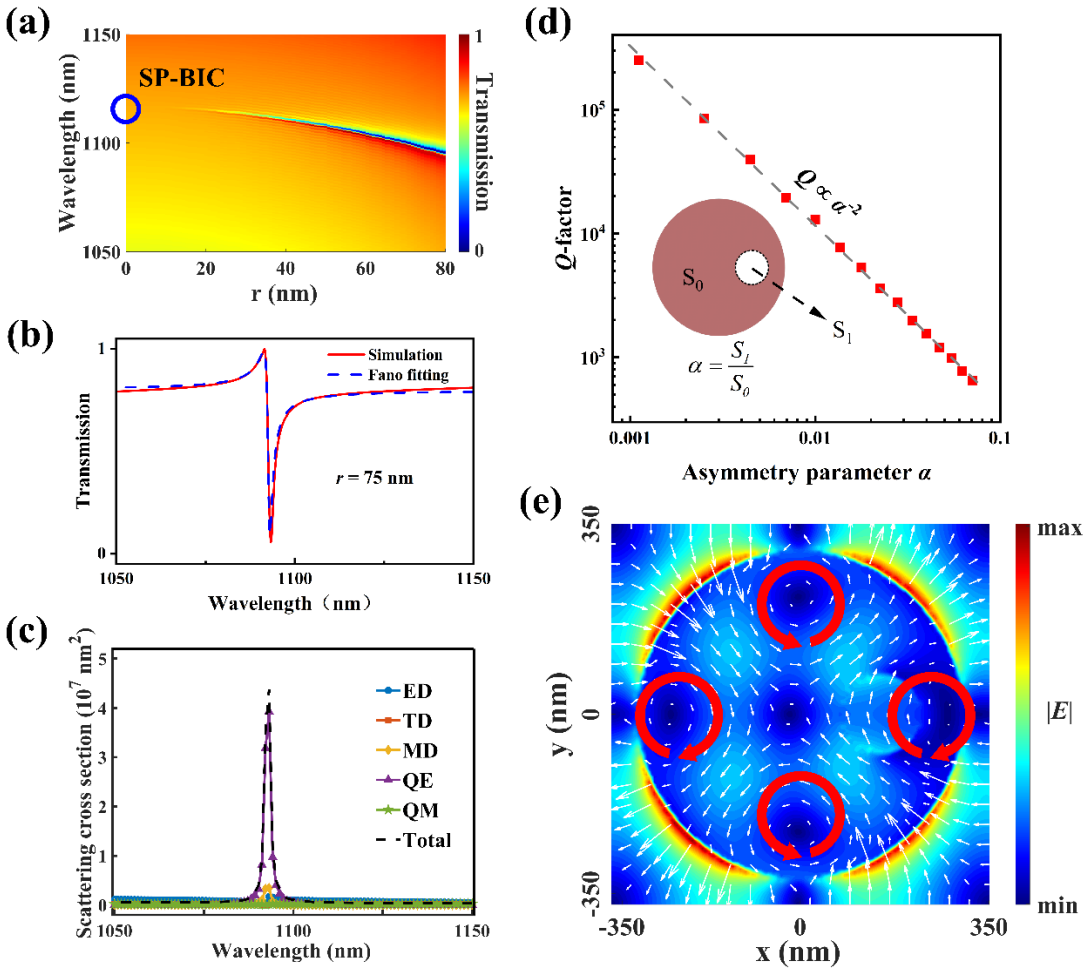

Fig. 3 (a) Transmission spectrum of the silicon nanodisk metasurface on a glass substrate relative to the radius of the eccentric hole, with the corresponding position of the SP-BIC marked by a basket circle. (b) Transmission spectrum at r = 75 nm and comparison with the fitted curve of the Fano formula. (c) Multilevel unfolding of the silicon metasurface resonance at r = 75 nm, shows the absolute dominance of the QE response at the resonance wavelength position. (d) The relationship between the Q-factor and the asymmetry parameter α, is plotted in logarithmic coordinates to visualize the relationship. (e) Image of the x-y plane electric field distribution at resonance for r = 75, with the red arrow indicating the direction of the in-plane displacement current.

3. Results and discussion

The wavelengths corresponding to the QBIC resonance modes supported by the proposed metasurface structures are in the NIR-II frequency range, and light waves in this range are commonly used for biological and medical detection. Usually, the resonance wavelength position of the metasurface structure also changes with the change of the surrounding dielectric constant, resulting in a redshift of the transmission spectrum as the effective refractive index increases[42]. Therefore, the study in this paper also has the potential to be used as a biosensor. Here, the effect on the QBIC resonance is first investigated by varying the refractive index of the background environment by simulation. The background in the standard condition is ideal air, so the background refractive index (noted as n_B) is set to $n_B = 1$. Here, the radius of the eccentric aperture is set to r = 35 nm, and according to the Q-α relationship in Fig. 3(d), the Q factor at this point can reach 8379. As shown in Fig. 4(a), there is a significant redshift of the transmission spectra as the background refractive index increases, which is attributed to the fact that an increase in the background refractive index leads to an increase in the overall effective refractive index of the metasurface structural unit. Here the background refractive index n_B varies between 1 and 1.40 and the refractive indices of many biological components are in this range. To investigate this property further, the position of the resonance peak wavelength in the transmission spectrum (referred to as λ_{dip})

ISSN 2616-5767 Vol.8, Issue 1: 73-80, DOI: 10.25236/AJETS.2025.080111

and the relationship between the full width at half maximum (referred to as FWHM) and n_B were analyzed and the results are shown in Figure 4(b). From the figure, it can be seen that there is a linear relationship between these two quantities and the background refractive index n_B and that the detection of the refractive index of biological components can be achieved using this linear dependence. Sensitivity S and Figure of Merit FOM are two important measures of sensor characteristics. For the refractive index sensor, the sensitivity S is defined as[43]:

$$S = \frac{\Delta\lambda}{\Delta n_B} \tag{4}$$

where $\Delta\lambda$ is the amount of change in the position of the resonance wavelength, Δn_B is the amount of change in the refractive index of the background, and S is in units of nm/ RIU. figure of merit FOM:

$$FOM = \frac{S}{FWHM} \tag{5}$$

Where FWHM is the full width at half maximum of the resonance peak of the transmission spectrum and FOM is in units of RIU^{-1}. Corresponding to the data in Figure 4(b), the performance of the sensor is characterized as S = 265.58 nm/RIU and FOM = 2178.31RIU^{-1}.

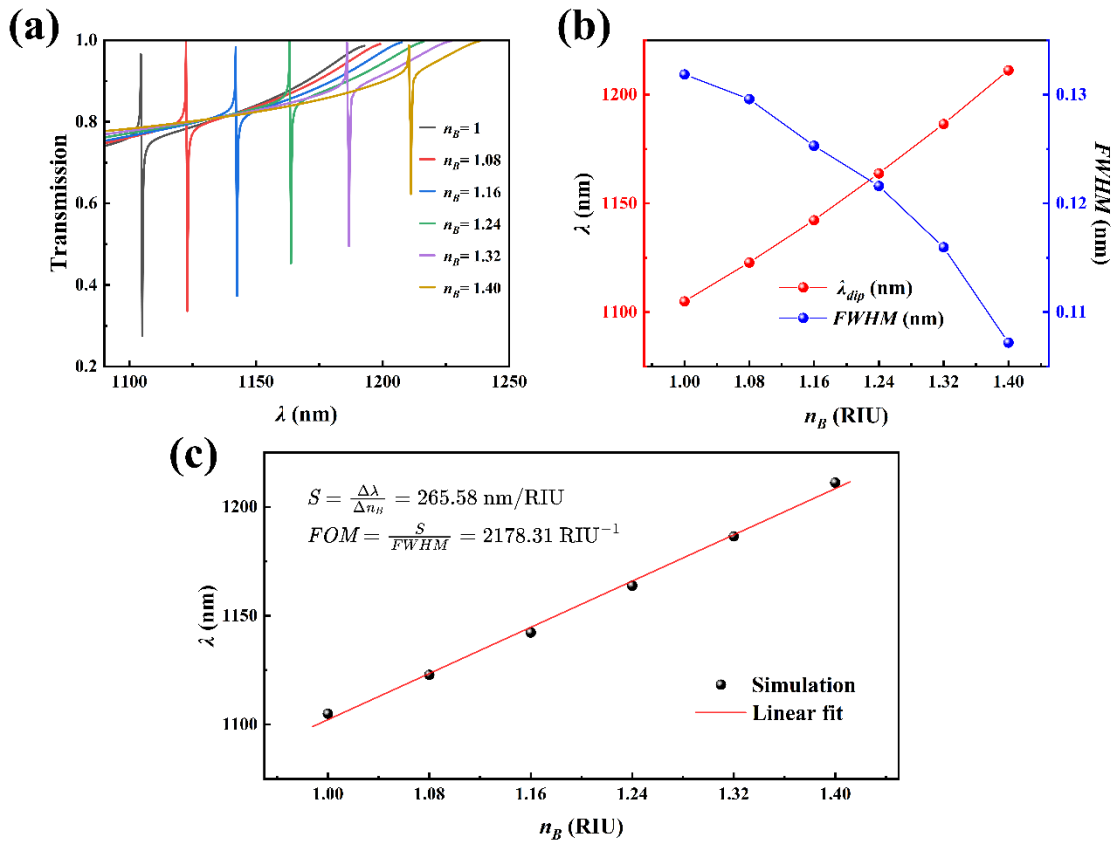

Fig. 4 (a) Transmission spectra at different background refractive indices. (b) Variation of resonance wavelength and full width at half maximum (FWHM) with background refractive index. (c) A linear fit to the variation of the resonance wavelength with background refractive index redshift. The sensitivity S and the figure of merit FOM are calculated from the fitted slope.

4. Conclusions

In summary, a novel all-dielectric metasurface structure is proposed to enable refractive index sensing with high sensitivity and accuracy. This metasurface consists of periodically arranged silicon wafers with eccentric holes on a glass substrate, which can support a symmetry-protected bound state in a continuous medium. When the in-plane symmetry of the metasurface is broken, the SP-BIC transforms into a QBIC

ISSN 2616-5767 Vol.8, Issue 1: 73-80, DOI: 10.25236/AJETS.2025.080111

with a high Q-factor, resulting in a Fano resonance with a sharp asymmetric line shape. The sensitivity of this resonance peak is very sensitive to changes in the surrounding refractive index and can therefore be used for accurate refractive index sensing. Based on the QBIC with a high Q-factor, this metasurface can achieve biological refractive index sensing with sensitivity and figure of merit of 265.58 nm/RIU and 2178.31 RIU^{-1}, respectively, which are higher than many existing studies. In addition to the high FOM sensing performance, this metasurface has lower ohmic loss and higher tunability compared to conventional plasma metasurfaces. As a result, this metasurface shows significant application potential for refractive index sensing measurements, offering higher detection sensitivity and broader applicability.

References

[1] Sadreev, A. F. (2021). Interference traps waves in an open system: bound states in the continuum. Reports on Progress in Physics, 84(5), 055901.
[2] Koshelev, K., Bogdanov, A., & Kivshar, Y. (2019). Meta-optics and bound states in the continuum. Science Bulletin, 64(12), 836–842.
[3] Tong, H., Liu, S., Zhao, M., & Fang, K. (2020). Observation of phonon trapping in the continuum with topological charges. Nature Communications, 11(1), 5216.
[4] Linton, C. M., & McIver, P. (2007). Embedded trapped modes in water waves and acoustics. Wave Motion, 45(1–2), 16–29.
[5] Marinica, D. C., Borisov, A. G., & Shabanov, S. V. (2008). Bound States in the Continuum in Photonics. Physical Review Letters, 100(18), 183902.
[6] Bulgakov, E. N., & Sadreev, A. F. (2008). Bound states in the continuum in photonic waveguides inspired by defects. Physical Review B, 78(7), 075105.
[7] Romano, S., Zito, G., Lara Yépez, S. N., Cabrini, S., Penzo, E., Coppola, G., Rendina, I., & Mocellaark, V. (2019). Tuning the exponential sensitivity of a bound-state-in-continuum optical sensor. Optics Express, 27(13), 18776.
[8] Srivastava, Y. K., Ako, R. T., Gupta, M., Bhaskaran, M., Sriram, S., & Singh, R. (2019). Terahertz sensing of 7 nm dielectric film with bound states in the continuum metasurfaces. Applied Physics Letters, 115(15), 151105.
[9] Liu, D., Wu, F., Yang, R., Chen, L., He, X., & Liu, F. (2021). Quasi-bound states in the continuum in metal complementary periodic cross-shaped resonators at terahertz frequencies. Optics Letters, 46(17), 4370–4373.
[10] Hsu, C. W., Zhen, B., Lee, J., Chua, S.-L., Johnson, S. G., Joannopoulos, J. D., & Soljačić, M. (2013). Observation of trapped light within the radiation continuum. Nature, 499(7457), 188–191.
[11] Koshelev, K., Favraud, G., Bogdanov, A., Kivshar, Y., & Fratalocchi, A. (2019). Nonradiating photonics with resonant dielectric nanostructures. Nanophotonics, 8(5), 725–745.
[12] Lee, J., Zhen, B., Chua, S.-L., Qiu, W., Joannopoulos, J. D., Soljačić, M., & Shapira, O. (2012). Observation and Differentiation of Unique High-Q Optical Resonances Near Zero Wave Vector in Macroscopic Photonic Crystal Slabs. Physical Review Letters, 109(6), 067401.
[13] Hsu, C. W., Zhen, B., Stone, A. D., Joannopoulos, J. D., & Soljačić, M. (2016). Bound states in the continuum. Nature Reviews Materials, 1(9), 1–13.
[14] Xu, L., Zangeneh Kamali, K., Huang, L., Rahmani, M., Smirnov, A., Camacho-Morales, R., Ma, Y., Zhang, G., Woolley, M., Neshev, D., & Miroshnichenko, A. E. (2019). Dynamic Nonlinear Image Tuning through Magnetic Dipole Quasi-BIC Ultrathin Resonators. Advanced Science, 6(15), 1802119.
[15] Paddon, P., & Young, J. F. (2000). Two-dimensional vector-coupled-mode theory for textured planar waveguides. Physical Review B, 61(3), 2090–2101.
[16] Bulgakov, E. N., & Sadreev, A. F. (2014). Robust bound state in the continuum in a nonlinear microcavity embedded in a photonic crystal waveguide. Optics Letters, 39(17), 5212–5215.
[17] Barrow, M., & Phillips, J. (2020). Polarization-independent narrowband transmittance filters via symmetry-protected modes in high contrast gratings. Optics Letters, 45(15), 4348–4351.
[18] Jain, A., Moitra, P., Koschny, T., Valentine, J., & Soukoulis, C. M. (2015). Electric and Magnetic Response in Dielectric Dark States for Low Loss Subwavelength Optical Meta Atoms. Advanced Optical Materials, 3(10), 1431–1438.
[19] Huang, L., Li, G., Gurarslan, A., Yu, Y., Kirste, R., Guo, W., Zhao, J., Collazo, R., Sitar, Z., Parsons, G. N., Kudenov, M., & Cao, L. (2016). Atomically Thin MoS2 Narrowband and Broadband Light Superabsorbers. ACS Nano, 10(8), 7493–7499.
[20] Wang, Y., Fan, Y., Zhang, X., Tang, H., Song, Q., Han, J., & Xiao, S. (2021). Highly Controllable Etchless Perovskite Microlasers Based on Bound States in the Continuum. ACS Nano, 15(4), 7386–7391.
[21] Chen, Y., Zhao, C., Zhang, Y., & Qiu, C. (2020). Integrated Molar Chiral Sensing Based on High-Q Metasurface. Nano Letters, 20(12), 8696–8703.

ISSN 2616-5767 Vol.8, Issue 1: 73-80, DOI: 10.25236/AJETS.2025.080111

[22] Alipour, A., Farmani, A., & Mir, A. (2018). High Sensitivity and Tunable Nanoscale Sensor Based on Plasmon-Induced Transparency in Plasmonic Metasurface. IEEE Sensors Journal, 18(17), 7047–7054. IEEE Sensors Journal.

[23] Kong, Y., Cao, J., Qian, W., Liu, C., & Wang, S. (2018). Multiple Fano Resonance Based Optical Refractive Index Sensor Composed Of Micro-Cavity and Micro-Structure. IEEE Photonics Journal, 10(6), 1–10.

[24] Bezus, E. A., Bykov, D. A., & Doskolovich, L. L. (2018). Bound states in the continuum and high-Q resonances supported by a dielectric ridge on a slab waveguide. Photonics Research, 6(11), 1084.

[25] Zeng, T.-Y., Liu, G.-D., Wang, L.-L., & Lin, Q. (2021). Light-matter interactions enhanced by quasi-bound states in the continuum in a graphene-dielectric metasurface. Optics Express, 29(24), 40177.

[26] Al-Ani, I. A. M., As'Ham, K., Huang, L., Miroshnichenko, A. E., & Hattori, H. T. (2021). Enhanced Strong Coupling of TMDC Monolayers by Bound State in the Continuum. Laser & Photonics Reviews, 15(12), 2100240.

[27] Xiang, J., Chen, J., Lan, S., & Miroshnichenko, A. E. (2020). Nanoscale Optical Display and Sensing Based on the Modification of Fano Lineshape. Advanced Optical Materials, 8(16), 2000489.

[28] Li, Z., Panmai, M., Zhou, L., Li, S., Liu, S., Zeng, J., & Lan, S. (2023). Optical sensing and switching in the visible light spectrum based on the bound states in the continuum formed in GaP metasurfaces. Applied Surface Science, 620, 156779.

[29] Wang, J., Kühne, J., Karamanos, T., Rockstuhl, C., Maier, S. A., & Tittl, A. (2021). All-Dielectric Crescent Metasurface Sensor Driven by Bound States in the Continuum. Advanced Functional Materials, 31(46), 2104652.

[30] Johnson, S. G., & Joannopoulos, J. D. (2001). Block-iterative frequency-domain methods for Maxwell's equations in a planewave basis. Optics Express, 8(3), 173–190.

[31] Xu, T., Wheeler, M. S., Nair, S. V., Ruda, H. E., Mojahedi, M., & Aitchison, J. S. (2008). Highly confined mode above the light line in a two-dimensional photonic crystal slab. Applied Physics Letters, 93(24), 241105.

[32] Yang, Z.-J., Hao, Z.-H., Lin, H.-Q., & Wang, Q.-Q. (2014). Plasmonic Fano resonances in metallic nanorod complexes. Nanoscale, 6(10), 4985–4997.

[33] Zong, X., Li, L., & Liu, Y. (2021). Photonic bound states in the continuum in nanostructured transition metal dichalcogenides for strong photon–exciton coupling. Optics Letters, 46(24), 6095–6098.

[34] Zhen, B., Hsu, C. W., Lu, L., Stone, A. D., & Soljačić, M. (2014). Topological Nature of Optical Bound States in the Continuum. Physical Review Letters, 113(25), 257401.

[35] Koshelev, K., Lepeshov, S., Liu, M., Bogdanov, A., & Kivshar, Y. (2018). Asymmetric Metasurfaces with High-Q Resonances Governed by Bound States in the Continuum. Physical Review Letters, 121(19), 193903.

[36] Limonov, M. F., Rybin, M. V., Poddubny, A. N., & Kivshar, Y. S. (2017). Fano resonances in photonics. Nature Photonics, 11(9), 543–554.

[37] Miroshnichenko, A. E., Flach, S., & Kivshar, Y. S. (2010). Fano resonances in nanoscale structures. Reviews of Modern Physics, 82(3), 2257–2298.

[38] Hinamoto, T., & Fujii, M. (2021). MENP: an open-source MATLAB implementation of multipole expansion for nanophotonics. OSA Continuum, 4(5), 1640–1648.

[39] Alaee, R., Rockstuhl, C., & Fernandez-Corbaton, I. (2018). An electromagnetic multipole expansion beyond the long-wavelength approximation. Optics Communications, 407, 17–21.

[40] Wang, X., Duan, J., Chen, W., Zhou, C., Liu, T., & Xiao, S. (2020). Controlling light absorption of graphene at critical coupling through magnetic dipole quasi-bound states in the continuum resonance. Physical Review B, 102(15), 155432.

[41] Li, Z., Xie, M., Nie, G., Wang, J., & Huang, L. (2023). Pushing Optical Virus Detection to a Single Particle through a High-Q Quasi-bound State in the Continuum in an All-dielectric Metasurface. The Journal of Physical Chemistry Letters, 14(48), 10762–10768.

[42] Zhou, C., Liu, G., Ban, G., Li, S., Huang, Q., Xia, J., Wang, Y., & Zhan, M. (2018). Tunable Fano resonator using multilayer graphene in the near-infrared region. Applied Physics Letters, 112(10), 101904.

[43] Guo, L., Zhang, Z., Xie, Q., Li, W., Xia, F., Wang, M., Feng, H., You, C., & Yun, M. (2023). Toroidal dipole bound states in the continuum in all-dielectric metasurface for high-performance refractive index and temperature sensing. Applied Surface Science, 615, 156408.